0273-2289/95/5503–0175$10.00

Periodic and Chaotic Behavior of Substrate-Inhibited Enzymatic Reactions with Hydrogen Ions Production

G. IBRAHIM,[1,2] F. A. TEYMOUR,[1,3] AND S. S. E. H. ELNASHAIE*,[1,4]

[1]Non-Linear Dynamics Group (NLDG), Chemical Engineering Department, King Saud University, Riyadh 11421, P.O. Box 800, Saudi Arabia; [2]Faculty of Engineering, Menofia University, Egypt; [3]Present address: Chemical Engineering Department, Illinois Institute of Technology, Chicago, IL; and [4]Chemical Engineering Department, Cairo University, Egypt

Received August 1, 1994; Accepted October 7, 1994

ABSTRACT

A two-compartment model of an enzyme system with substrate inhibition kinetics and hydrogen ion production is investigated. The model is used to study the bifurcation, instability, and chaotic behavior of the system. The investigation, although in a restricted region of the parameters' space, has uncovered a good part of the rich dynamic characteristics of this system, including: period doubling sequences leading to chaos, banded chaos, fully developed chaos, interior crisis, tangent bifurcation leading to intermittency, periodic windows interrupting chaotic regions, and alternating periodic chaotic sequences. The results relate to the phenomena occurring in physiological experiments, such as the periodic stimulation of neural cells and the voltage-gated ion channel dynamics.

Index Entries: Enzyme systems; substrate-inhibition; acetylcholinesterase; bifurcation; chaos.

*Author to whom all correspondence and reprint requests should be addressed.
e-mail: F45K006@SAKSVOO.BITNET.

Abbreviations: A_m, active membrane area m^2; B_h, V_m, V_m E $V_1/(K_h \cdot q)$ (dimensionless); B_s, V_m E $V_1/(K_s \cdot q)$ (dimensionless); f, refer to feed conditions; H, hydrogen ions; h, dimensionless concentration of hydrogen ions; K_s, K_i, K_h, K'_h, constants characteristic the enzyme; K_w, equilibrium constant of water ($Kmol^2/m^6$); OH, hydroxyl ions; q, volumetric flow rate (m^3/s); P_1, choline $[HO(CH_2)N^+(CH_3)_3]$; P_2^-, acetate (CH_3COO^-); R, rate of reaction $Kmol/m^3$ s; R_w, rate of water formation $Kmol/m^3$ s; r, dimensionless rate of reaction; S, substrate; s, dimensionless substrate concentration; T, $t.q/V_1$ dimensionless time; V_m, maximum reaction rate (Kmol/Kmol·s); V_1, V_2, volume of compartments (1) and (2); α'_H, membrane permeability for hydrogen ions (m/s); α_H, dimensionless membrane permeability for hydrogen ions $[\alpha'_{OH}A_m/q]$; α'_s, membrane permeability for substrate (m/s); α_s, dimensionless permeability for substrate (α'_s A_m/q); α'_{OH}, membrane permeability for hydroxyl ions (m/s); α_{OH}, dimensionless permeability for hydroxyl ions $[\alpha'_{OH}$ $A_m/q]$; α_i, dimensionless substrate inhibition constant $[K_s/K_i]$; δ, K_h/K'_h; γ, K_w/K_{h2}.

INTRODUCTION

Achieving a theoretical understanding of nerve excitation is a central problem of theoretical biophysics (*1–8*). With the accumulating knowledge regarding enzyme kinetics, it is reasonable to expect that a theory explaining electrical behavior in some of the enzyme systems might be extended to apply to natural excitable membranes (*7,9*).

The enzyme system under consideration in the present study is inhibited by substrate and is affected by the production of the hydrogen ions accompanying the reaction. An example of such enzyme is the acetylcholinesterase, which produces choline and acetic acid (which is fully ionized to acetate ions and H^+) from acetylcholine substrate. This enzyme plays a recognized role in nerve excitation (*10*). Acetylcholine is secreted by neurons in many areas of the brain, but specifically by the large pyramidal cells of the motor cortex, and by many different neurons that innervate the skeletal muscles. A significant portion of this enzyme is found in intercellular compartments (*11*). In most cases, acetylcholine has excitatory effects (*10*).

In enzyme membrane systems, the local production of hydrogen ions decreases the pH, and owing to the amphoteric properties of the proteinaceous membrane, the lower the pH, the lower the density of the negative fixed charges in the membrane (*12*). Local pH changes inside an artificial enzyme membrane were first shown by Goldman et al. (*13*). The potential differences resulting from acetylcholine when injected on one side of an artificial acetylcholinesterase membrane exhibit a similar electrical response to the behavior observed with excitable membranes (*9*). The steady-state potential resulting from the enzyme activity for increasing and decreasing substrate concentrations exhibits a hysteresis behavior. Because of the

autocatalytic effect resulting from the production of hydrogen ions and the existence of diffusional resistances, hysteresis phenomenon develops in a definite range of parameters. Because of the amphoretic properties of the membrane, the hysteresis of the internal pH is transformed into a hysteresis in membrane potential (*9*). In addition, the nonmonotonic behavior of the enzyme reaction rate coupled with the diffusion constraints causes instabilities and oscillatory behavior in membrane potential and in acetylcholine concentration level.

The two-compartment model used in this investigation is represented by four coupled differential equations, and therefore, chaotic behavior of the system is possible since it is known that chaotic behavior is only possible with systems having dimensions higher than two.

The phenomenological model used in this study differs greatly from other membrane excitation models, such as the Rose-Hindmarsh model of action potential (*14,15*), which is a modification of the Fitzhugh model (*16*). This later model was developed in order to simulate the repetitive, patterned, and irregular activity seen in molluscan neurons. The work of Holden and Fan (*17–20*) on the dynamic behavior of membrane excitation using this three-variable model of action potential shows clearly the existence of different dynamic modes, including simple periodic, bursting periodic, and chaotic behavior. A wealth of transition mechanisms between different types of behavior have been discovered by Holden and Fan (*17–20*). These mechanisms include period doubling, boundary crises, period adding, saddle-node tangent bifurcation, and saddle-node nontangent bifurication. It is interesting to notice that many of the dynamic phenomena discovered by Holden and Fan (*17–20*) using the three-dimensional nonphenomenological action potential Rose-Hindmarsh model are also obtained using the present phenomenological two-compartment model with membrane separating the two compartments.

The understanding of excitable membrane behavior is strongly related to the advances in the mathematical theory of bifurcation, as well as the advances in chemical and biochemical engineering research in this field. Bifurcation and instability have attracted great attention in the last 20 years, and excellent reviews for the bifurcation of chemically reactive systems have been published (*21,22*). With the discovery of chaotic behavior in the dynamics of different physical systems, research in the field of dynamic bifurcation of chemically reactive systems has taken a great leap forward. Complex dynamic behavior, including chaotic behavior of various reactive systems, has been investigated by many researchers in different fields of physical sciences (*23–36*).

In life sciences, the hopes of ecologists for many years concentrated on trying to explain the population dynamics of plants and animals in terms of simple and stable interactions among species. In the mid-1970s, it was discovered that even simple interactions may result in chaotic population dynamics (*37*). Furthermore, Hassell and coworkers (*38*) have shown that interactions among species may lead not only to dynamic

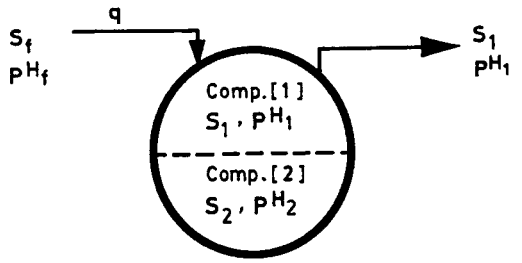

Fig. 1. The two-compartment model.

chaotic behavior, but also to chaotic patterns in space where population booms and busts occur in seemingly random patterns (*39–44*).

Despite the extensive research carried out to study the complex dynamics of chemical, biochemical, biological, and medical reactive systems (*45–47*) and the extensive efforts expended to generalize some of the results, it seems that only a part of the tip of the iceberg has been uncovered so far. The present article is an additional modest contribution to these efforts. In the present article, a simple two compartment model is used to investigate the complex behavior of an enzyme system inhibited by substrate and affected by the production of hydrogen ions (i.e., acetylcholinesterase) when the enzyme exists free in solution in each compartment. The problem had been tackled in much simpler form by El-Nashaie and coworkers (*42,48,49*) almost ten years ago when only static bifurcation has been investigated. In light of the relatively recent advances in fundamental knowledge and techniques regarding such dynamical systems, the problem is revisited on a higher level of model formulation and analysis of the results, and a wealth of new dynamic features are discovered that make the results of the earlier investigation no more than a scratch on the surface of the problem.

MATHEMATICAL FORMULATION OF THE PROBLEM

The problem investigated is that of the enzymatic reaction:

$$S \xrightarrow{E} P_1 + P_2^- + H^+$$

where in the case of acetylcholinesterase; S denotes acetylcholine [$CH_3CO.O(CH_2)_2\ N^+(CH_3)_3$], P_1 denotes choline [$HO(CH_2)_2\ N^+(CH_3)_3$], and P_2^- denotes acetate (CH_3COO^-).

The reaction is considered to take place in a constant-flow, isothermal, continuous stirred-tank reactor (CSTR) divided by a semipermeable membrane into two compartments as shown in Fig. 1. The reaction takes place in the liquid phase according to the following rate equation (*42*):

$$R(S,H) = V_m(S) / \{(S) + (S)^2/K_i + K_s[K_h + (H) + (H)^2/K'_h]/(H)\} \quad (1)$$

where (S) is the substrate concentration, (H) is the hydrogen ion concentration, V_m is the maximum reaction rate per unit mass of enzyme; K_s, K_h, and K'_h are equilibrium constants, and K_i is an inhibition constant. If the active volume of the compartments are V_1 and V_2, the enzyme concentrations in both compartments are equal to E in units of enzyme mass per unit of active volume, and the volumetric flow rate is q, then the material balance equations for the two compartments can be written as follows.

Hydrogen ion unsteady-state mass balance gives:

$$V_j \cdot d(H_j)/dt = a_{1j} \cdot q \cdot [(H_f) - (H_1)] - a_{2j} \cdot \alpha'_H \cdot A_m [(H_1) - (H_2)] + V_j \cdot R_j (S, H) \cdot E - V_j \cdot R_{wj} \quad (2)$$

where $j = 1$ and 2 denotes compartments 1 and 2, respectively; $a_{11} = 1$, $a_{12} = 0$, $a_{21} = -1$, $a_{22} = -1$; (H_f) is the concentration of hydrogen ions in the feed and R_{wj} is the rate of water formation in compartment j. The parameter α'_H is the membrane permeability of hydrogen ions, and A_m is the active membrane area.

Hydroxyl ion unsteady-state mass balance gives:

$$V_j \cdot d(OH_j)/dt = a_{1j} \cdot q \cdot [(OH_f) - (OH_1)] - a_{2j} \cdot \alpha'_{OH} \cdot A_m [(OH_1) - (OH_2)] - V_j \cdot R_{wj} \quad (3)$$

where (OH_f) is the concentration of hydroxyl ions in the feed and α'_{OH} is the membrane permeability for hydroxyl ions.

Substrate unsteady-state mass balance gives:

$$V_j \cdot d(S_j)/dt = a_{1j} \cdot q \cdot [(S_f) - (S_1)] - a_{2j} \cdot \alpha'_s \cdot A_m [(S_1) - (S_2)] - V_j \cdot R_j (S,H) \cdot E \quad (4)$$

The pseudo-steady-state assumption for hydroxyl ions gives:

$$d(OH)/dt = 0 \quad (5)$$

If it is also assumed that hydrogen and hydroxyl ions are at equilibrium, we obtain the following relation

$$K_w = (H)(OH) \quad (6)$$

where K_w is the equilibrium constant of water. Subtracting Eq. (3) from Eq. (2) and substituting from Eqs. (5) and (6) into Eq. (2) gives:

$$V_j \cdot d(H_j)/dt = a_{1j} \cdot q \cdot [(H_f) - (H_1)] - K_w [1/(H_f) - 1/(H_1)] - a_{2j} [\alpha'_H \cdot A_m [(H_1) - (H_2)] - K_w \cdot \alpha'_{OH} \cdot A_m [1/(H_1) - 1/(H_2)] + V_j \cdot R_j (S,H) \cdot E \quad (7)$$

Equation (7) can be written in the following dimensionless form:

$$dh_j/dT = a_{1j}(h_f - h_1) - b_j \cdot \alpha_H (h_1 - h_2) - a_{1j} \cdot \gamma \cdot (1/h_f - 1/h_1) + B_h \cdot r_j + b_j \cdot \gamma \cdot \alpha_{OH} (1/h_1 - 1/h_2) \quad (8)$$

where $b_1 = 1$, $b_2 = -V_R$, $V_R = V_1/V_2$, $h = (H)/K_h$, $B_h = V_m E V_1/(K_h \cdot q)$, $\gamma = K_w/K_h^2$, $\alpha_H = \alpha'_H \cdot A_m/q$, $\alpha_{OH} = \alpha'_{OH} \cdot A_m/q$, and $T = t \cdot q/V_1$.

and

$$r_j = s_j / [s_j + s_j^2 \cdot \alpha_i + (1 + h_j + h_j^2 \cdot \delta)/h_j] \tag{9}$$

where $s = (S)/K_s$, $\alpha_i = K_s/K_i$, and $\delta = K_h/K'_h$.

The substrate balance (Eq. [4]) can also be written in dimensionless form as follows:

$$ds_j/dT = a_{1j}(s_f - s_1) - b_j \alpha_s (s_1 - s_2) - B_s \cdot r_j \tag{10}$$

where $\alpha_s = \alpha'_s A_m/q$ and $B_s = V_m E V_1/(K_s \cdot q)$.

The two-compartment model is thus represented by the four differential equations 8, 10 (with $j = 1, 2$) with four state variables, h_1, h_2, s_1, and s_2, which describe the dynamics of hydrogen ions and substrate in the two compartments.

NUMERICAL TOOLS AND PRESENTATION TECHNIQUES

The methodology used consists of the numerical continuation techniques, coupled with the principles of bifurcation theory. The bifurcation diagrams are obtained using the software package AUTO 86 of Doedel (*50*). This package is able to perform both steady-state and dynamic bifurcation analysis, including the determination of entire periodic solution branches. AUTO also computes the Floquet multipliers along periodic solution branches and, therefore, determines the stability of the periodic orbits. A periodic orbit loses its stability by a number of mechanisms. The most common of them are period doubling bifurcation and saddle-node tangent bifurcation. Because of periodicity, there is always a Floquet multiplier equal to +1. When Floquet multipliers lie inside the unit circle, the periodic solution is asymptotically stable. Complex Floquet multipliers indicate node or saddle-like bifurcation. A Floquet multiplier leaving the unit circle through −1 indicates period doubling bifurcation. Passage of complex Floquet multipliers out of the unit circle indicates that the periodic orbit bifurcates to an invariant torus. When a Floquet multiplier leaves the unit circle through +1, the stable periodic orbit (node) collides with another unstable orbit (saddle), and both orbits evaporate. This is called saddle-node bifurcation. Hopf bifurcation (HB) points and periodic limit (PLP) points are degenerate points because they have two Floquet multipliers equal to +1.

The Dassel subroutine (*51*), with automatic step size to ensure accuracy, is used for numerical simulation of periodic as well as chaotic attractors. The differential equations of the present system are quite stiff, and in many cases, a bound on allowable error as small as 10^{-15} was necessary to obtain accurate results. The classical time trace and phase plane presentations for the dynamics are used. However, for high periodicity and

chaotic attractors, these techniques are not sufficient, and therefore, other presentation techniques are used. These techniques are based on the plotting of discrete points of intersection (Return points) between the trajectories and a hyperplane (Poincare surface). These discrete points of intersection are taken such that the trajectories intersect the hyperplane transversally and cross it in the same direction. Accurate numerical techniques are used for interpolation to obtain the exact return points in order not to introduce external noise into the results.

The return points are used to construct a number of important diagrams:

1. Poincare bifurcation diagram: a plot of one of the coordinates of the return points (e.g., pH_1) vs a bifurcation parameter (e.g., s_f);
2. Return point histogram: a plot of one of the coordinates of the return points vs time (dimensionless time T);
3. Return points iterate maps of different order: a two-dimensional plot of one of the coordinates of the n-th return point vs the coordinates of $(n + i)$-th return points. The iterate maps are first order, second order, third order, ...when $i = 1, 2, 3...$, and
4. Two dimensional Poincare map: a plot of two of the coordinates of the return points (e.g., pH_1 and pH_2) for a specific value of the bifurcation parameter (s_f).

THE TWO-PARAMETER CONTINUATION AND THE CHOICE OF α_s, α_H, α_{OH}, V_R, and pH_f

Figure 2A is a two-parameter continuation diagram for the two parameters α_s and s_f showing the loci of the HB points. There is one degenerate HB point (a) where the transversality condition of the definition of the HB point (*52*) is violated (the conditions for the crossing of the imaginary axis by the eigenvalues), that is:

$$|\{ d\, Re[\mu(\alpha_s)] / d\, \alpha_s \}|\, \alpha_{so} = 0 \qquad (11)$$

which means that the derivative of the real part of the eigenvalue $Re[(\mu(\alpha_s)]$ with respect to a bifurcation parameter α_s is equal to zero at this HB point α_{so}. It is well known that complex behavior usually occurs in the vicinity of such degenerate HB points (*52*). The value of α_s is chosen in the vicinity of point (a) in the region where four HB points exist. A two-parameter continuation of α_H *vs* s_f is shown in Figure 2B, and α_H is chosen in the vicinity of the degenerate HB point (A) in Fig. 2B, where there are also four HB points. Figure 2C is a two-parameter continuation for α_{OH} vs s_f for the above-chosen value of α_H. The ratio between hydrogen and hydroxyl ion permeabilities gives a value of α_{OH} of 0.5, which is in the vicinity of the degenerate HB point (a). Figure 2D is a two-parameter continuation

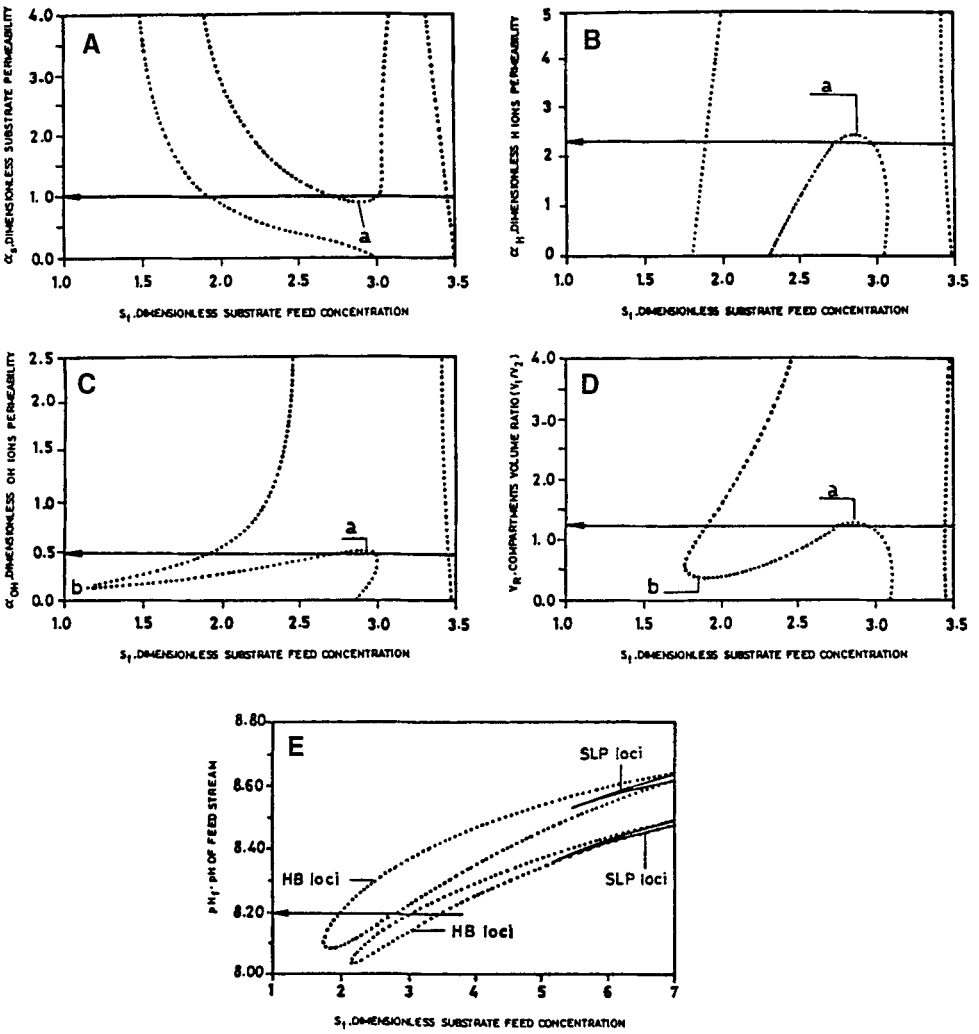

Fig. 2. Two-parameter continuation diagrams for the loci of HB points: (**A**) α_S, dimensionless substrate permeability vs s_f. (**B**) α_H, dimensionless H^+ ions permeability vs s_f. (**C**) α_{OH}, dimensionless OH ion permeability vs s_f. (**D**) V_R, dimension-less compartments volume ratio vs s_f. (**E**) pH_f, pH of feed stream vs s_f.

for V_R vs s_f, in the vicinity of the degenerate HB points (a). Figure 2E is a two-parameter continuation for pH_f vs s_f. On this diagram, two types of loci are plotted. The dotted curves are for the HB, and the solid curves are for the static limit points (SLP) (another type of degeneracy is apparent in the top right part, which results from the intersection of the loci of HB and SLP curves). In this article, this second type of degeneracy is avoided, and pH_f is chosen away from this degeneracy in a region with four normal Hopf bifurcation points. The rest of the parameters (γ, α_i, δ, B_h, B_s) are chosen at the values that were used earlier by El-Nashaie et al. (42). Table 1 shows the base set of the system of parameters used in this investigation.

Table 1
Base Set of Parameters

Parameter	Value	Remarks
B_h	50	Ref. (42)
B_s	100	Ref. (42)
δ	0.1	Ref. (42)
α_i	0.5	Ref. (42)
γ	0.01	Ref. (42)
α_s	1.0	
α_H	2.25	
α_{OH}	0.5	
V_R	1.2	
pH_f	8.2	

"The Two-Parameter Continuation and the Choice of α_S, α_{OH}, V_R, and pH_f" in this article.

RESULTS AND DISCUSSION

In all the results presented, the substrate feed concentration s_f is used as the bifurcation parameter, and all the presentation techniques discussed earlier are utilized to investigate the rich dynamic behavior of the system.

Static and Dynamic Bifurcation Diagrams

Figure 3A shows the bifurcation diagram for a very wide range of the bifurcation parameters (s_f). This case is characterized by the existence of four HB points at low substrate concentrations ($3.508 > s_f > 1.998$) and a small region of multiplicity of steady states at high substrate concentrations ($32.8 < s_f < 34.8$). The four HB points are connected with two periodic branches as shown in the enlargement of box a (Fig. 3B). The periodic branch connecting HB_2 and HB_3 is unstable, whereas the branch connecting HB_1 and HB_4 points is stable, except for the small region in the neighborhood of HB_4 (box b). Box b of Fig. 3B is enlarged as shown in Fig. 3C. One of the interesting phenomenon observed is the occurrence of bistability in the region between HB_2 and HB_3 where a periodic and a point attractor coexist with unstable limit cycles acting as separatrices, separating the domains of attraction of the periodic and point attractors. This bistability causes the interesting phenomenon that at the same values of s_f, different initial conditions lead to different attractors. Figure 4 (A and B) shows the time trace curves for the same parameters and fixed value of the bifurcation parameter ($s_f = 2.83$) for two different initial conditions. It is clear that small changes in initial conditions give rise to different attractors, one periodic and the other a fixed-point attractor. In biological sciences, the domain of attraction of the point attractor is usually called the blackhole (53). If a perturbation is introduced into the system when it

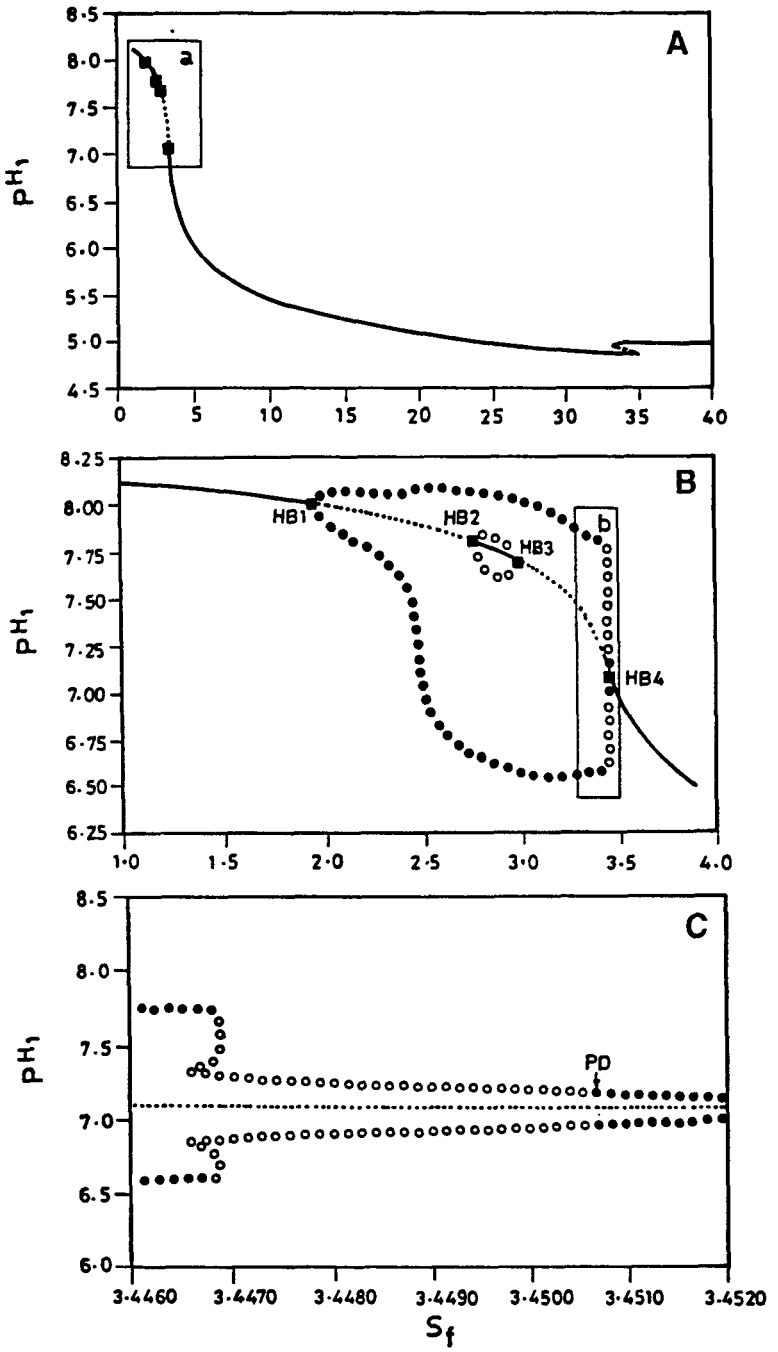

Fig. 3. Bifurcation diagrams of pH_1 vs s_f: (**A**) Overall diagram. (**B**) Enlargement of the box (a). (**C**) Enlargement of the rectangular (b). (____ Stable static branch, --- unstable static branch, o o o stable periodic branch, ooo unstable periodic branch.)

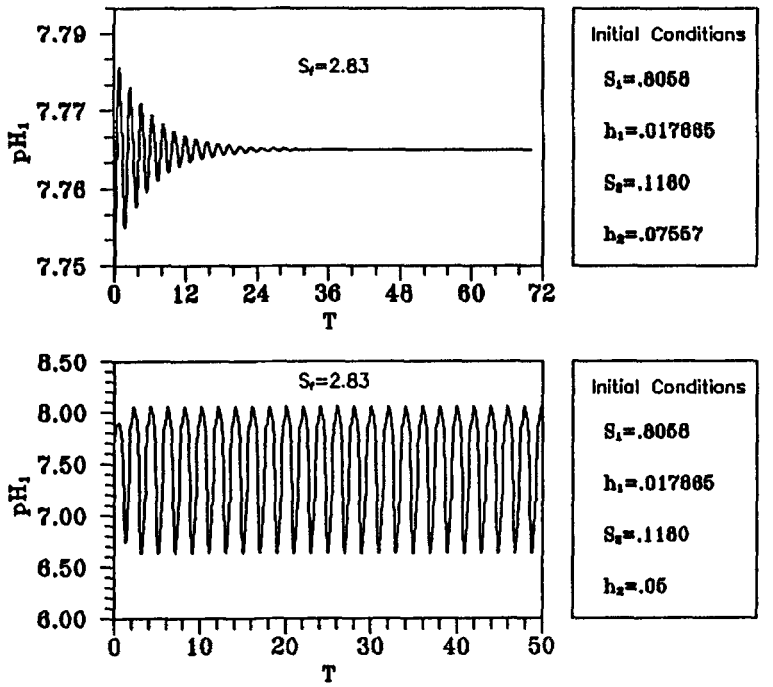

Fig. 4. Dynamic characteristics at s_f = 2.83 for two different initial conditions.

is attracted on the periodic attractor, it would be possible to break the stable periodic attractor, and push it out of its domain of attraction and into the blackhole, resulting in the annihilation of the oscillation.

Figure 5 (A and B) show the time trace (pH_1 vs T) and the phase plane (pH_2 vs pH_1) for the period one oscillation at s_f = 3.45063 (very close to the period doubling point on the right-hand side of Fig. 6), whereas Fig. 5 (C and D) shows the same for the period one attractor on the left-hand side of Fig. 6. It is clear that the amplitudes of pH_1 and pH_2 oscillation are different in the two different sides of Fig. 6. They are large (hard oscillation) on the left-hand side, and small (soft oscillation) on the right-hand side, with the chaotic region and its windows lying in the region of s_f between the two different types of oscillation.

Figure 5D shows an interesting feature with regard to the difference between the pH values in compartments 1 and 2, pH_1 and pH_2, respectively:

$$\Delta pH = pH_2 - pH_1$$

It is clear from Fig. 5D that ΔpH changes its sign twice during each cycle (period), which means that the H^+ ions transfer between the two compartments and change their direction twice every cycle. This alternating sign of ΔpH is associated with the hard oscillations in Figs. 5A and B. The two modes of sustained oscillations observed in this very narrow region of the

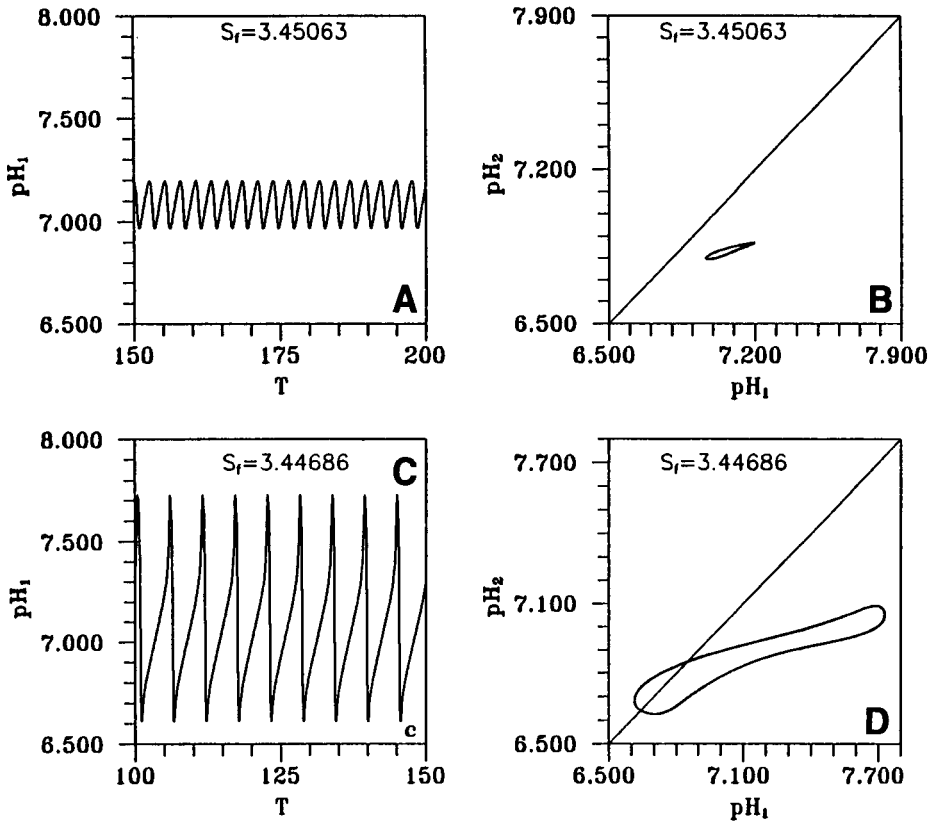

Fig. 5. Dynamic characteristics for two of the points edging the whole chaotic region (s_f = 3.45063 and s_f = 3.44686).

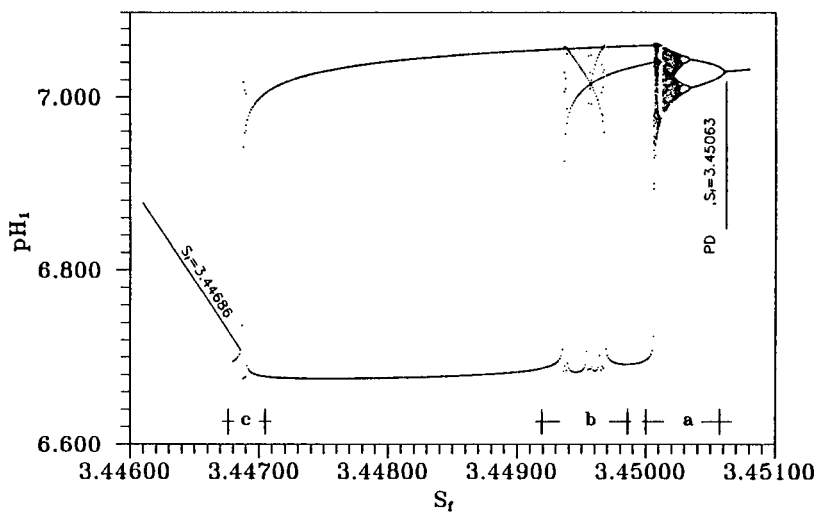

Fig. 6. One-dimensional Poincare bifurcation diagram covering all the region under investigation (intersections with the Poincare plane at s_1 = 0.37).

change of s_f may give some insight into the common physiological phenomenon of slow wave rhythm of membrane potential that characterizes the self-excitation of some of the smooth muscles owing to the acetylcholine-acetylcholinesterase activity (*10*). The cause of slow wave rhythm is as yet unknown; one suggestion is that the permeability of the membrane increases and decreases rhythmically (*10*). The mode of small-amplitude oscillations proved to be an intrinsic characteristic of the enzyme system under investigation and may be responsible for such rhythmicity in vivo, since the rhythmicity in H^+ ions may create its own potentials or play a basic role in controlling the voltage-gated ion channels of cell membranes.

The alternating change in the sign of ΔpH related to the enzyme activity (change in the direction of H^+ ions transfer) may be one of the possible mechanisms of action potentials responsible for the contraction of some smooth muscles. It is known that action potentials change their sign from negative mV values to positive mV values (*10*), which may correlate to the change in sign in ΔpH associated with the hard oscillation mode observed in this investigation. The importance of slow waves lies in the fact that they can initiate action potentials. The slow waves themselves cannot cause muscle contraction, but when the potential of the slow wave rises above a certain level (threshold potential), an action potential develops (*10*).

The transition from the large-amplitude oscillation, which is shown in Fig. 5C, to the relatively small-amplitude oscillations (Fig. 5A) is quite complex. This can be elucidated using Fig. 6, which is the one-dimensional Poincare bifurcation diagram of the state variable pH_1 vs the bifurcation parameters s_f. The range of s_f in this figure covers the gap between the pD point at $s_f = 3.450629$ and the point of $s_f = 3.44686$ shown in Fig. 3C. From Fig. 6, the following characteristics are evident:

1. With decreasing s_f, the periodic branch with P_1 (low-amplitude oscillation) originating from HB_4 goes through a sequence of period doubling (P_1, P_2, P_4, P_8. . .) leading to chaos. This chaotic behavior undergoes a number of bifurcations from chaos to periodicity and vice versa. Globally speaking, the range terminates at the point $s_f = 3.44686$ and a periodic branch with P_1 (large-amplitude oscillation) is born.
2. With the decrease of s_f and on the scale of Fig. 6, some periodic windows are observed: windows of periods four, five, and three in addition to the relatively wide range of P_2 window; and
3. On the left-hand side of Fig. 6, these are P_1 attractors. Then with increasing s_f, a very thin strip of chaos is encountered. This strip of chaos bifurcates to a relatively wide range of P_2 attractors. The clearly visible periodic windows of Fig. 6 seem to be dividing the diagram into regions of different chaotic densities.

CHAOTIC ATTRACTORS AND THE CONNECTION BETWEEN CHAOTIC AND PERIODIC ATTRACTORS

So far, we have used AUTO together with very limited reference to the results of numerical simulation presented phase plane, time trace and a one-dimensional Poincare bifurcation diagram to cover some of the dynamic characteristics of the system. The remaining gaps in the investigation can be approached by the use of numerical simulation and a set of presentation techniques (Poincare maps, return points of iterate maps of different orders, and return points histograms, in addition to the classical phase planes and time traces).

The Poincare bifurcation diagram for the whole region in the case under investigation is shown in Fig. 6. On this scale, we can only observe that a period doubling sequence leading to chaos emanates from the periodic branch, which originates from HB_4, and that the gaps between the stable periodic windows are interrupted by chaos. In order to achieve better visualization and analysis of this complex region in a well-organized and detailed fashion, this complex region is divided into three subregions, a, b, and c, as shown in Fig. 6.

Region A

This region is enlarged in Fig. 7. It covers an important part of the neighborhood of HB_4 point, and covers the heavy density chaotic regions in Fig. 6. With the decrease of s_f (from right to left), the P_1 periodic branch starting at HB_4 loses its stability through a period doubling sequence, and a stable P_2 attractor is born. The period doubling sequence continues giving P_2, P_4, P_8, P_{16}... until a four-banded chaos starts after four interior crises points take place. The four-banded chaos disappears where two interior crises take place at $s_f = 3.450253$ to give two-banded chaos. The two chaotic bands exist until the interior crises point $s_f = 3.450217$. After that, a fully developed chaos is observed. Figure 8 shows clearly the characteristics of the two-band chaos. Figure 8C is the return-point histogram. It shows clearly the existence of two chaotic bands. Figure 8A shows that the return points on the two-dimensional Poincare map (pH_1 vs pH_2) are concentrated in two disconnected segments; the same is observed in Fig. 8B, which presents the return point iterate map of order one. The phase plane (Fig. 8D) and the time trace (Fig. 8E) also support the existence of two-band chaos. This two-band chaos terminates at the interior crises point $s_f = 3.450217$, and a fully developed chaos is observed. Figure 9 shows clearly the characteristics of the fully developed chaos. It is clear that the unconnected segments of the Poincare maps are now connected (Fig. 9 [A and B]); the two heavy density zones of the phase plane in the two-band case are now mixed as shown in Fig. 9D. Also the return points are mixed in the return-point histogram as shown in Fig. 9C. The time trace curve shows the irregular oscillations in this case. However, the

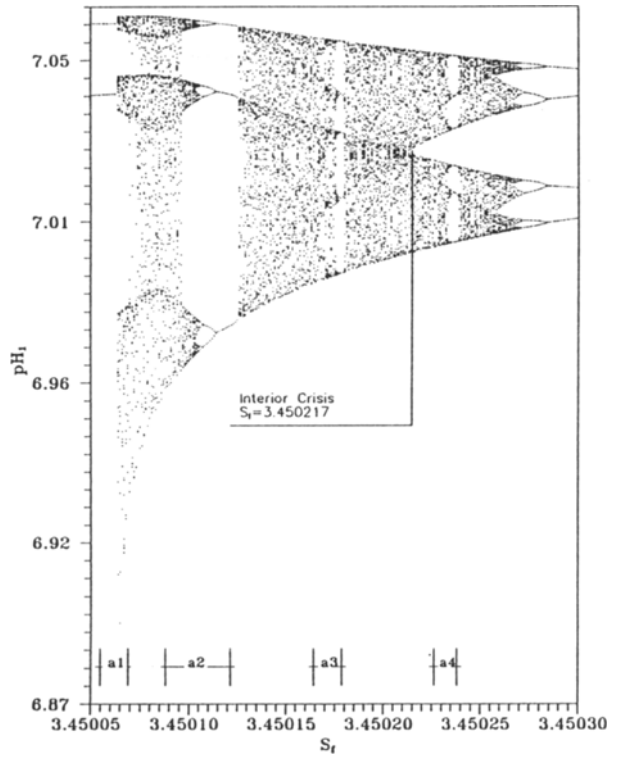

Fig. 7. Enlargement of section (a) of Fig. 6: period doubling cascade to fully developed chaos.

oscillations are still of small amplitude in comparison with the large-amplitude oscillations characterized the periodicity of s_f = 3.44686 (Fig. 5C).

Near the end of this zone and at s_f = 3.450127, the fully developed chaos turns to intermittency and eventually loses its stability to a P_3 stable attractor creating a P_3 window as shown in Fig. 10 (section a_2 in Fig. 7). Pomeau and Manneveille (*54*) proposed that chaotic attractors can lose their stability through intermittency (tangent bifurcation). The term intermittency refers to oscillations that are periodic for certain intervals (laminar phase) interrupted by intermittent erratic bursts of periodic oscillations of finite duration. After the bursts, the system returns to the laminar phase again until the next episode occurs. This intermittent behavior is shown for s_f = 3.450127 in Fig. 11. It is clear in Fig. 11 (A and C) that the dynamics alternate between regions of P_3 and chaos. The sequence of the third iterate maps in Fig. 11 (D, E, and F) makes this fact clearer: the curve approaches the diagonal, almost becoming a tangent at three distinct points as the enlargements of box i in Fig. 11E and box k in Fig. 11F. It is these small gaps that creates the three laminar channels giving rise to intermittency.

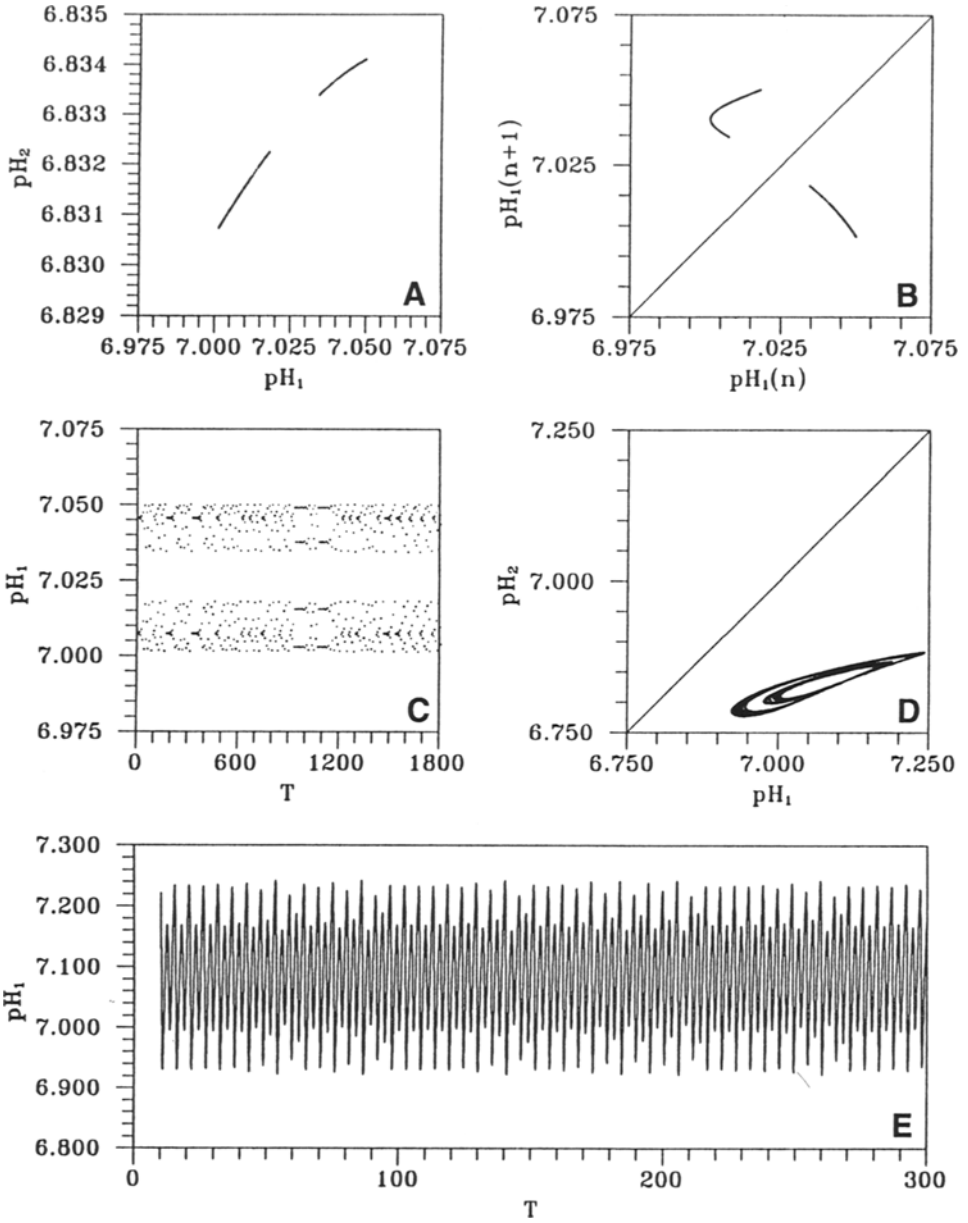

Fig. 8. Detailed dynamic characteristics of the two-band chaos at s_f = 3.450255. (**A**) Two-dimensional Poincare map (pH_1 vs pH_2 of the return points). (**B**) Return-point iterate map of order one. (**C**) Return-point histogram. (**D**) Phase plane. (**E**) Time trace.

As soon as the curve touches the diagonal and then intersects it, the intermittency disappears and a P_3 stable attractor is born, together with a P_3 unstable orbit. The P_3 attractor goes through period doubling sequence to chaos (P_3–P_6–P_{12}... chaos) as s_f decreases. The resulting chaos is banded (three bands), and at certain interior crisis points, it becomes a

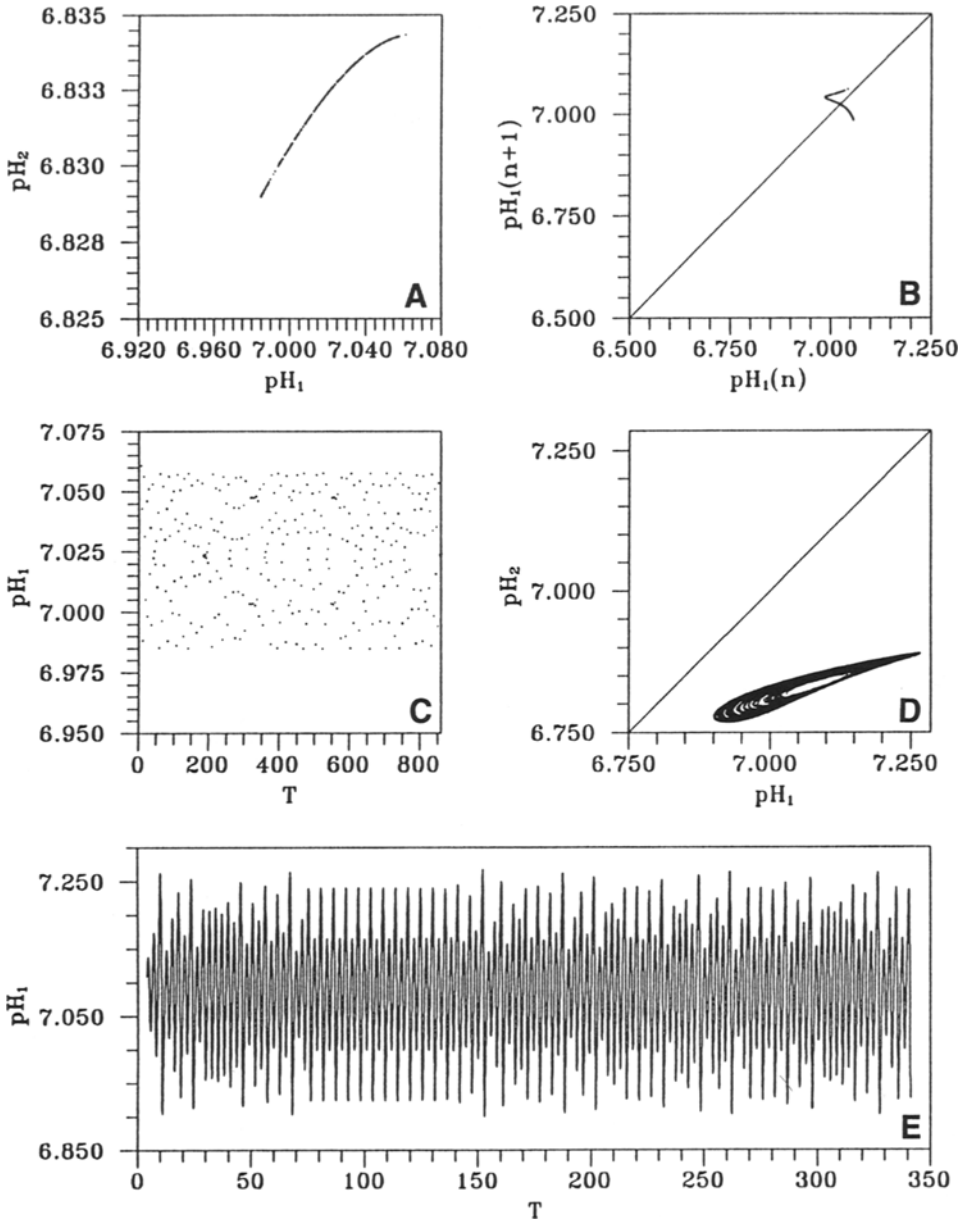

Fig. 9. Detailed dynamic characteristics of fully developed chaos at s_f = 3.45015. (**A**) Two-dimensional Poincare map. (**B**) Iterate map of order one. (**C**) Return-point histogram. (**D**) Phase plane. (**E**) Time trace.

fully developed chaos. Figure 12 shows the three-band chaos. It is clear that the return points concentrated in three disconnected segments as shown in Fig. 12 (A and B). The return-point histogram in Fig. 12C clearly shows the existence of three bands. Also, the phase plane is characterized by three heavy density zones as shown in Fig. 12D; the time trace also

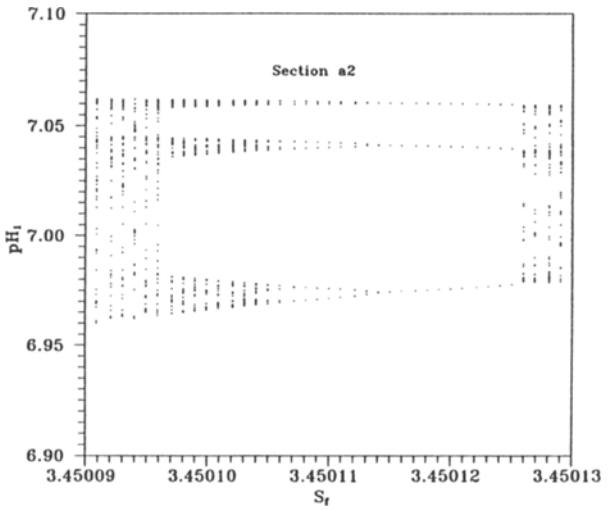

Fig. 10. Enlargement of section (a_2) in Fig. 7.

supports the existence of three-band chaos as shown in Fig. 12E. The three-band chaos turns to fully developed chaos with the decrease in s_f; s_f ϵ (3.45007, 3.450096). Near the end of this zone, as shown in Fig. 13A (this figure represents section a_1 of Fig. 7) and at s_f =3.4500702, the fully developed chaos turns to intermittency and eventually loses its stability to a P_6 stable attractor creating a P_6 periodic window as shown in Fig. 13B. This intermittent behavior is shown for s_f = 3.4500702 in Fig. 14. The sequence of 6th iterate maps in Fig. 14A and the enlargements i and k in Fig. 14 (B and C) show the existence of this intermittent behavior: the curve approaches the diagonal, almost becoming a tangent at six distinct points and creating six laminar channels giving rise to intermittency. The return-point histogram in Fig. 14D makes this fact clearer. Fig. 14 (E and F) shows the time trace and the phase plane for this intermittent chaos. The P_6 attractor goes through period doubling sequence to three-band chaos as s_f decreases where s_f ϵ (3.4500624, 3.4500695). Near the end of this zone and at s_f = 3.4500624, the three-band chaos turns to intermittency again and loses its stability to a P_3 attractor. Figure 15 shows this intermittent behavior. The third iterate map makes this fact clear. Periodic windows of odd and even periodicities are also noticed as shown in Figs. 10 and 13B, where the P_3 window and P_6 window are observed. Figures 16 and 17 show the P_5 window and P_6 window, respectively (Fig. 16 represents section a_3 in Fig. 7 and Fig. 17 represents section a_4).

Figure 18 shows the dynamics of two points. One of them is located just before the beginning of region a from left at s_f = 3.45006, and the second point is located at the entrance of the chaotic zone from the left-hand side at s_f = 3.4500634. It is clear that for s_f = 3.45006, the exchangeable feature of the pH differences (ΔpH) is still evident, and the amplitude of the oscillations is still large, whereas this feature disappears for the chaotic attractor at the second s_f = 3.4500634.

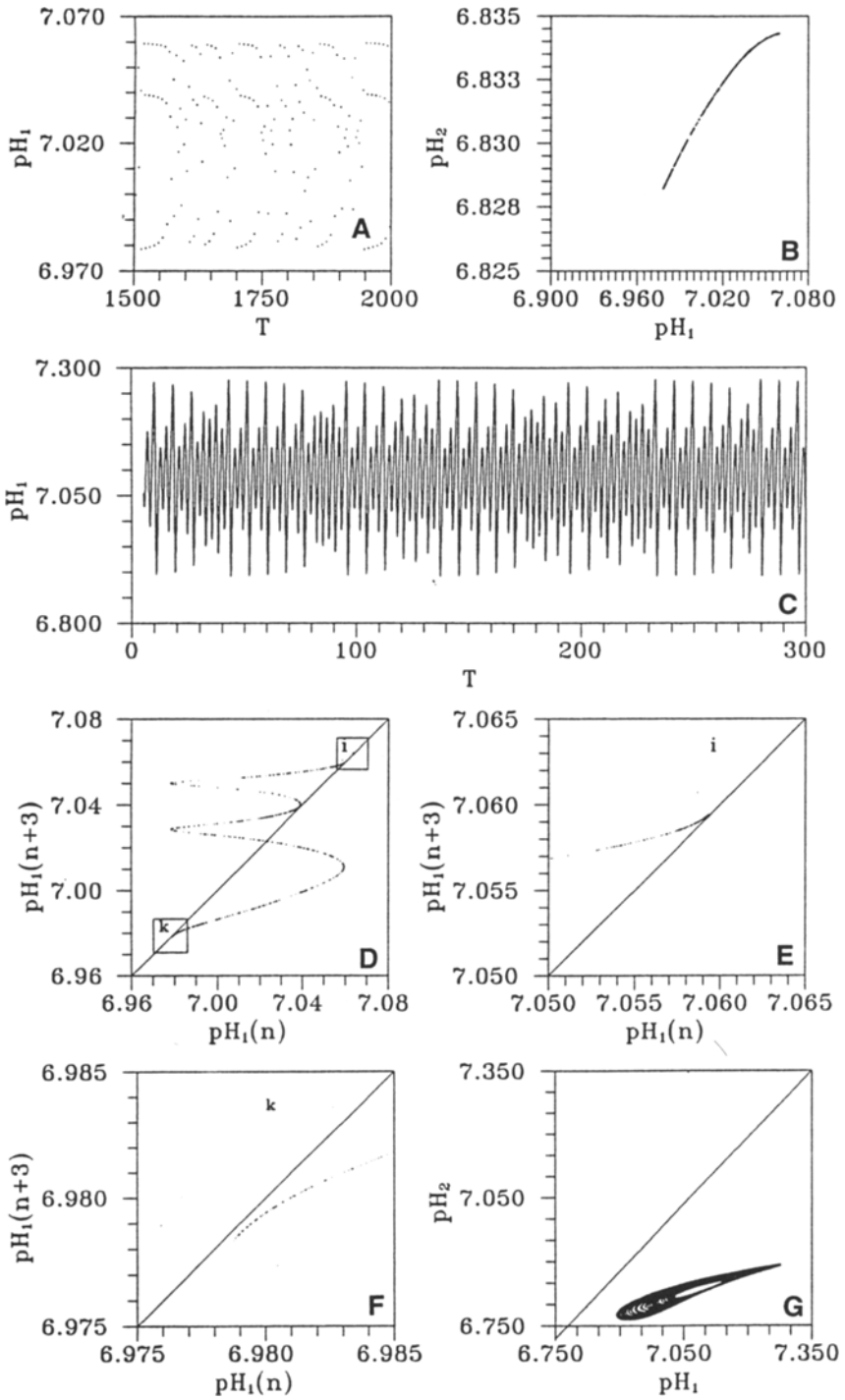

Fig. 11. Detailed dynamic characteristics of intermittent chaos at s_f = 3.450127: (**A**) Return-point histogram. (**B**) Two-dimensional Poincare map. (**C**) Time trace. (**D**) Return-point third iterate map. (**E**) Enlargement of box i. (**F**) Enlargement of box k. (**G**) Phase plane.

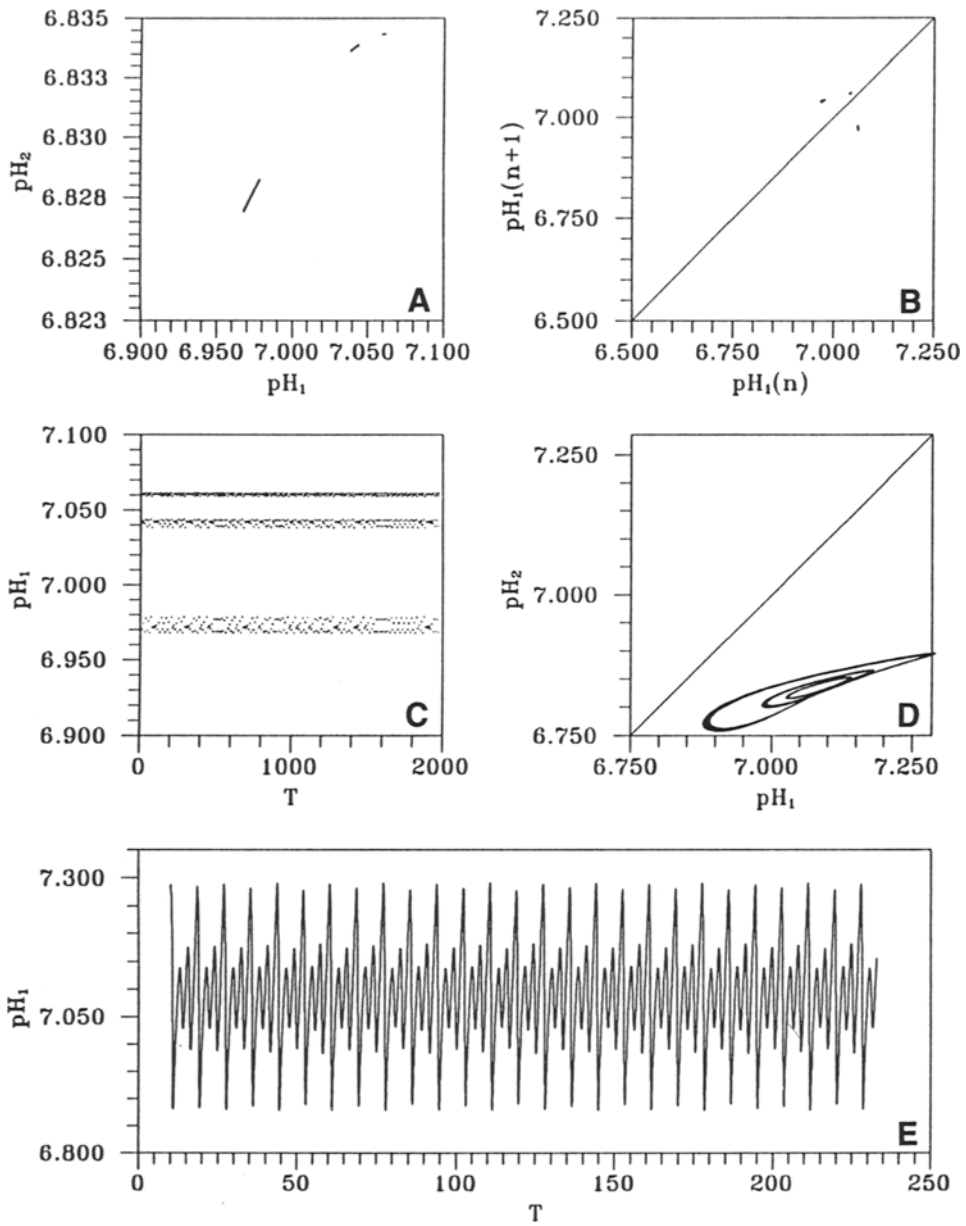

Fig. 12. Detailed dynamic characteristics of s_f = 3.4500103 (three-band chaos): (**A**) Two-dimensional Poincare map. (**B**) Return-point first iterate map. (**C**) Return-point histogram. (**D**) Phase plane. (**E**) Time trace.

Region B

This region is shown in Fig. 19 where $s_f \in (3.4493, 3.4499)$. This region covers the transition from the P_2 window to the P_3 window emerging from the heavy-density chaotic zone. As s_f increases, it is noticed that four periodic windows P_2–P_4–P_5–P_3 exist and that four chaotic regions inter-

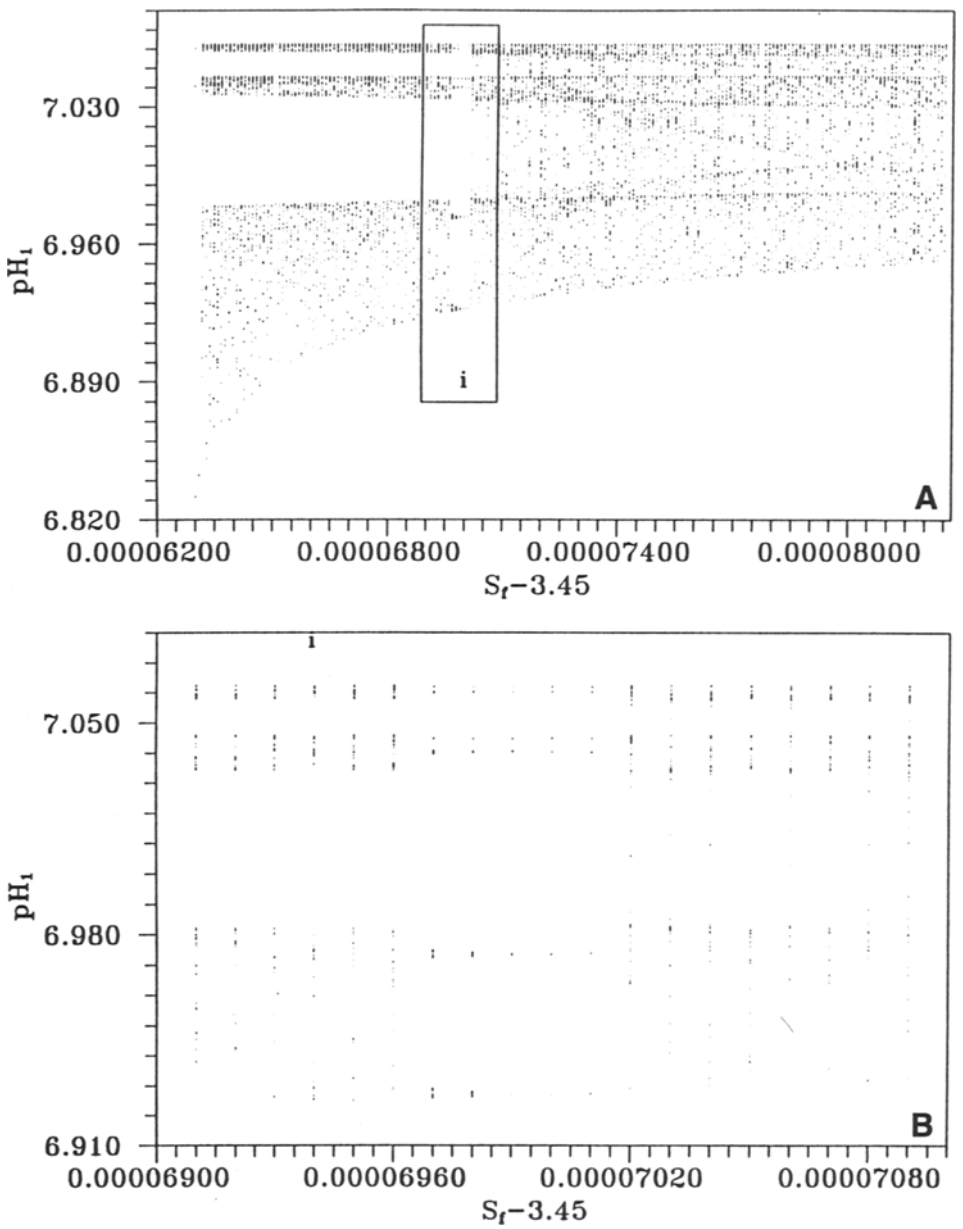

Fig. 13. (**A**) Enlargement of section (a_1) in Fig. 7. (**B**) Enlargement of box i.

rupt these four periodic windows. Figure 20 shows the dynamic behavior of each of the observed four periodic windows.

Region C

This is the last region where $s_f \in (3.44686, 3.44691)$. It is clear that the thin chaotic strip observed in the scale of Fig. 6 is much more complex, and the P_3 window bounded by two chaotic strips is observed on the scale

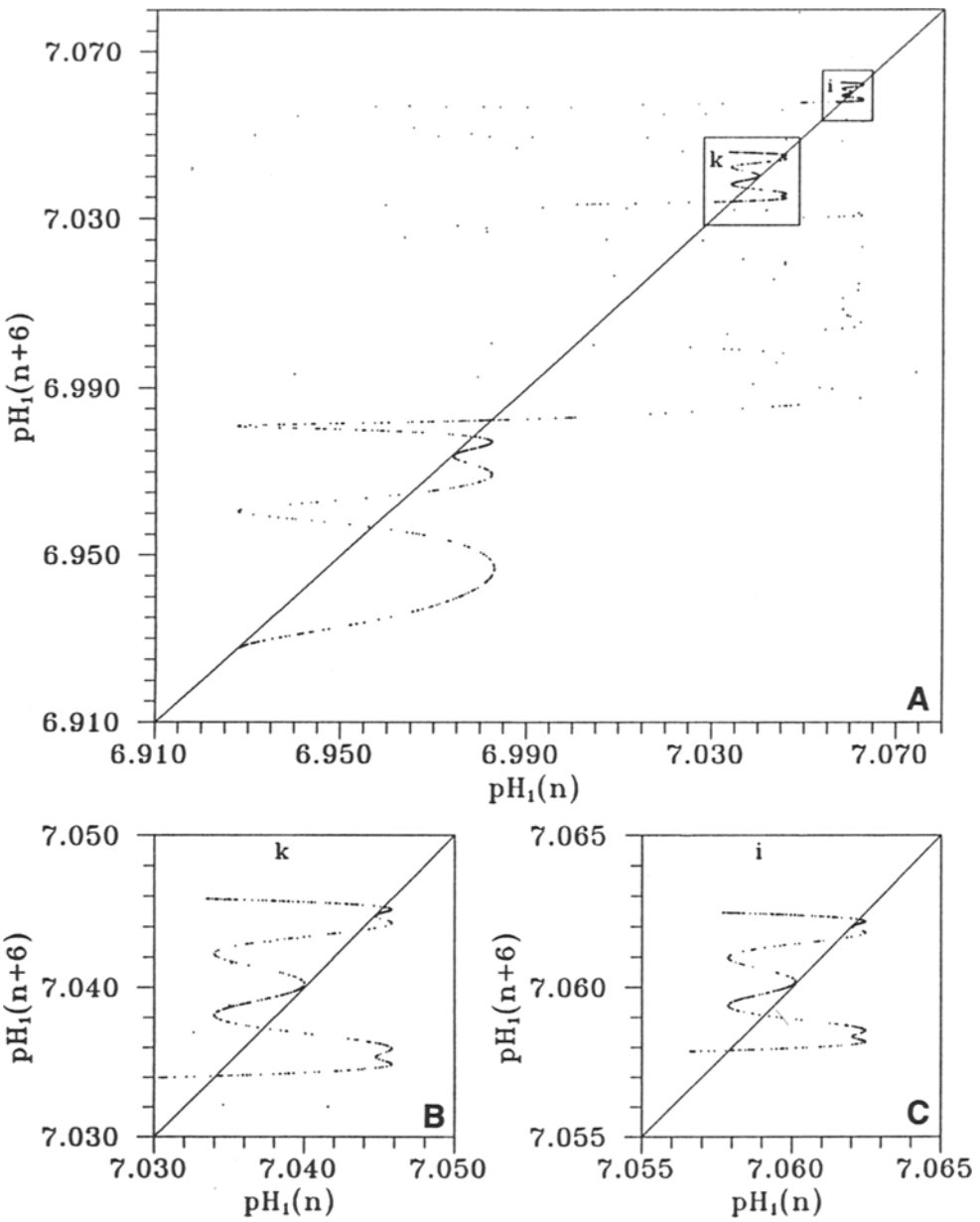

Fig. 14. Detailed dynamic characteristics at s_f = 3.4500702 (intermittent chaos): (**A**) Return-point iterate map of six order. (**B**) Enlargement of box k. (**C**) Enlargement of box i. (**D**) Return-point histogram. (**E**) Time trace. (**F**) Phase plane.

of Fig. 21A. Figure 21 (B–G) shows the dynamics of the three zones separating the two thin chaotic strips: P_1, P_3, P_2.

In general, in all the regions discussed, the transition from the small-amplitude oscillations to the large-amplitude oscillations proved to be through a chaotic region. Also, as Fig. 18 shows, theirs is a threshold value

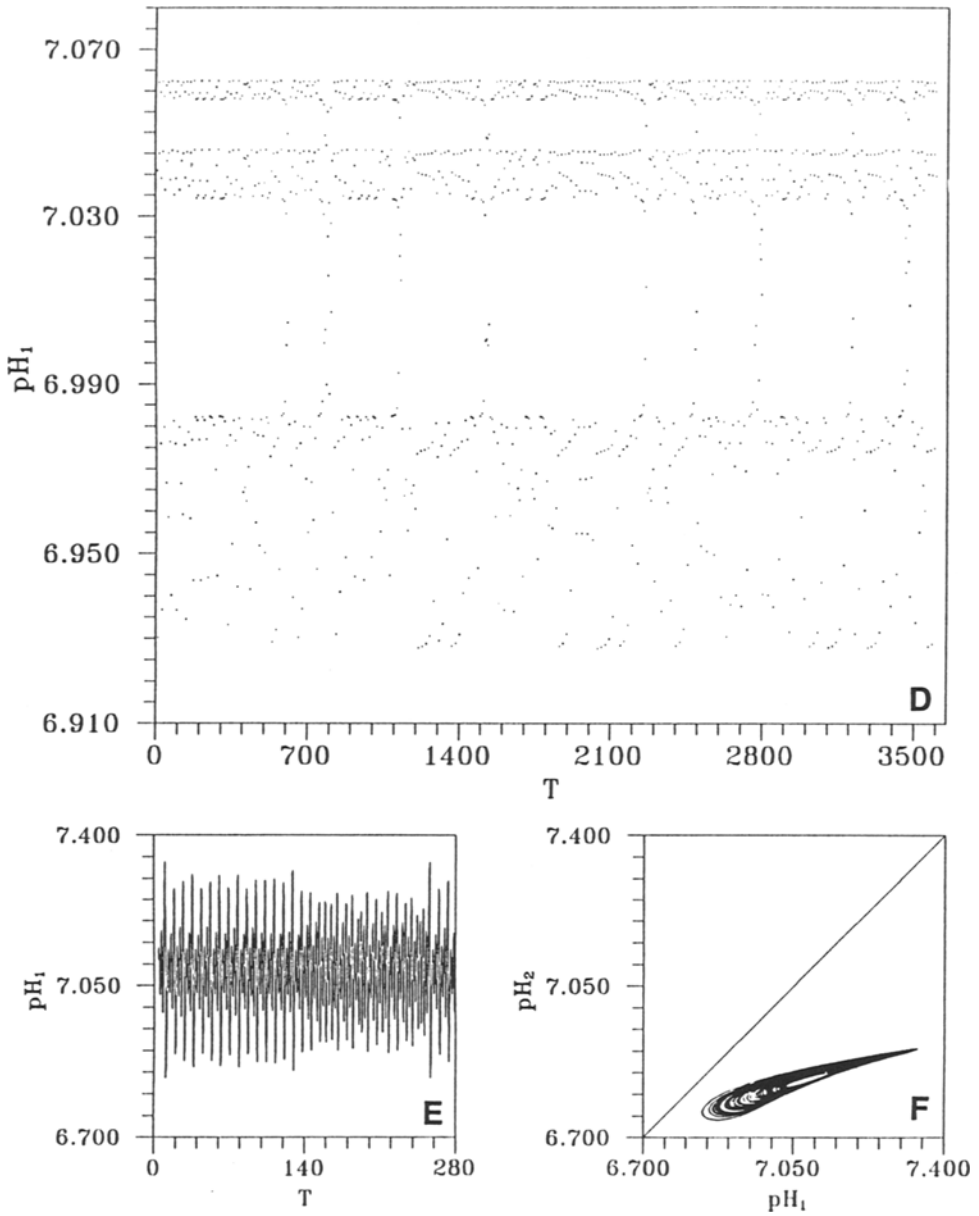

Fig. 14. (cont'd).

of s_f (3.45006) at which the small-amplitude oscillations of chaotic nature bifurcate to a periodic large-amplitude oscillation having the feature of alternating pH difference. This may correlate to the self-transition of the slow wave oscillation to action potentials through a threshold value of slow wave potentials in some of the smooth muscles. Also, different oscillation modes investigated in this study may serve as gating function (*55*); that is, all the oscillation modes of potential differences that come as a

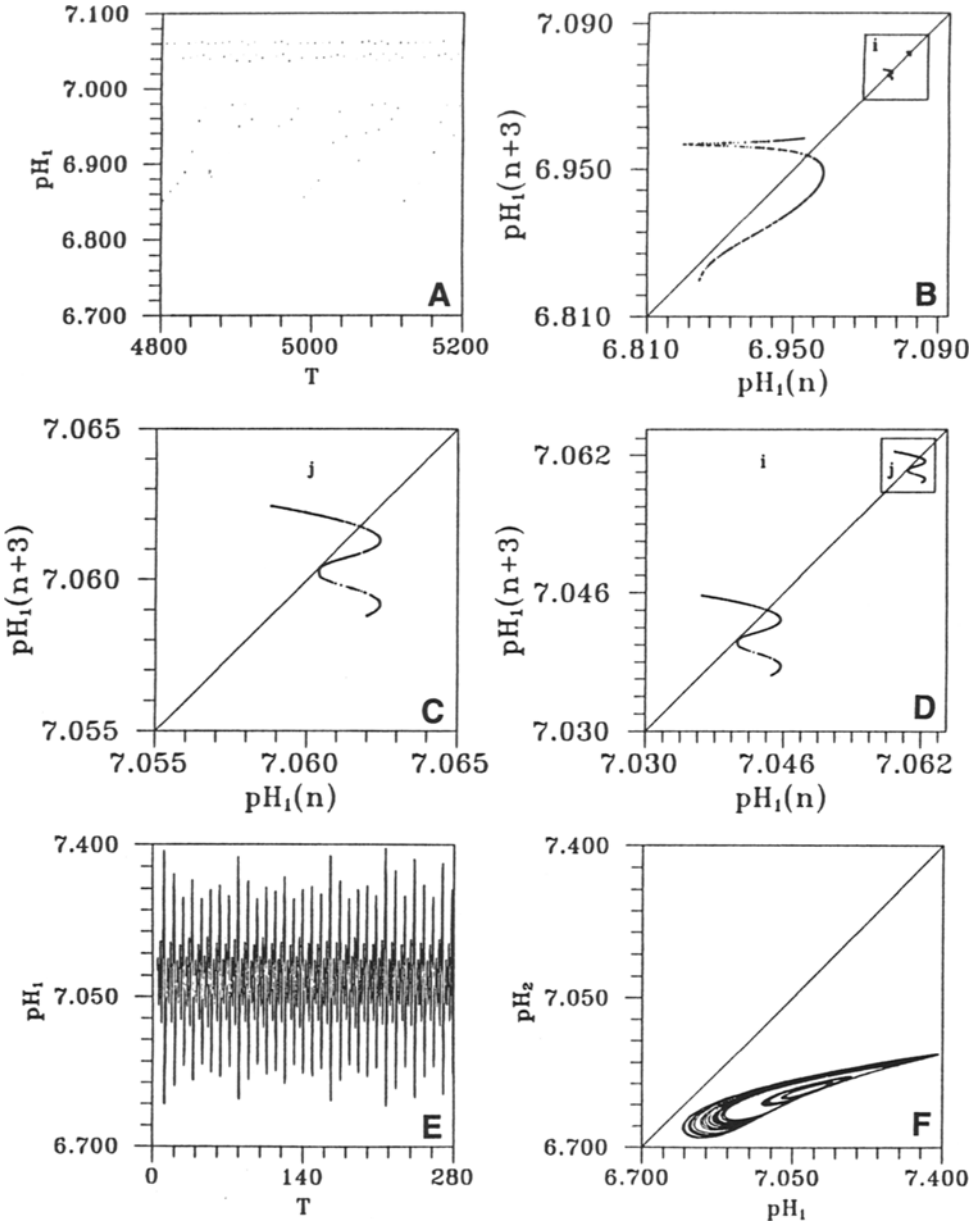

Fig. 15. Detailed dynamic characteristics at s_f = 3.4500624 (intermittent chaos): (**A**) Return-point histogram. (**B**) Return-point third iterate map. (**C**) Enlargement of box j. (**D**) Enlargement of box i. (**E**) Time trace. (**F**) Phase plane.

result of the H^+ ions' oscillatory behavior should play a significant role in controlling the voltage-gated ion channels in the cell membrane.

New evidence that certain types of neurons have "intrinsic oscillatory behavior" that may underlie rhythmic electroencephalography activities was discussed by Lopes-da-Silva (*55*); an excellent review of the applica-

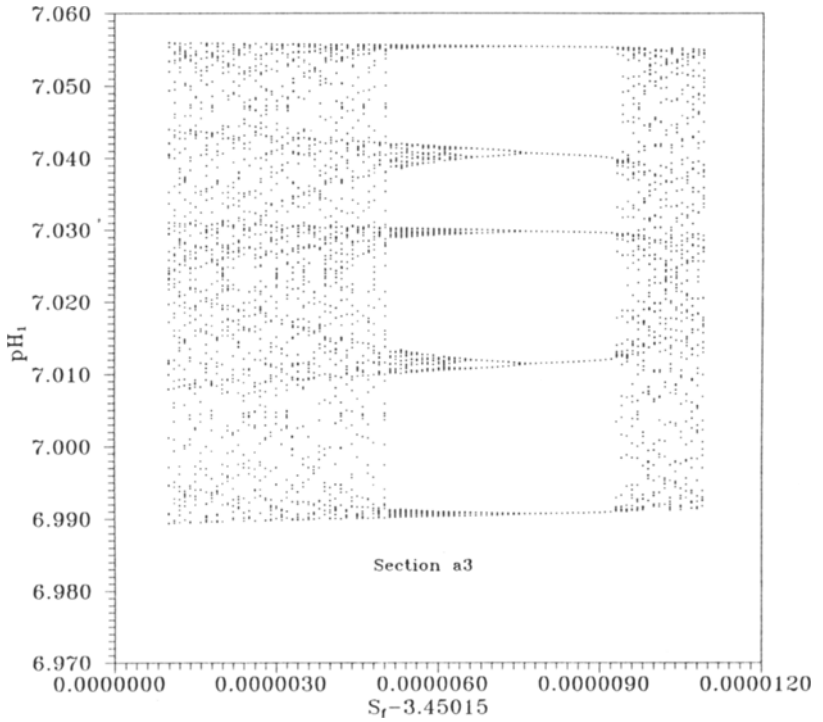

Fig. 16. Enlargement of section (a_3) in Fig. 7.

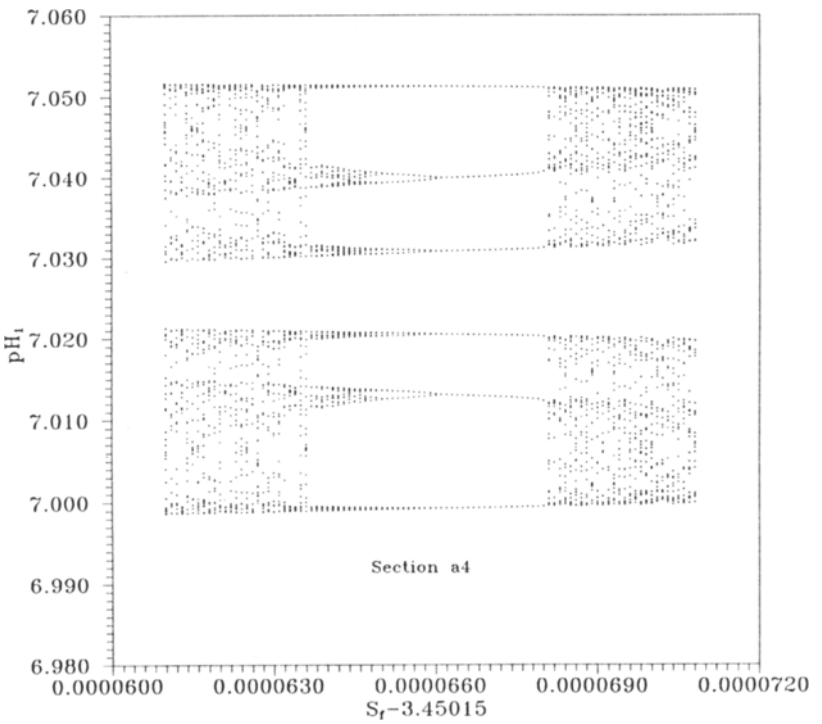

Fig. 17. Enlargement of section (a_4) in Fig. 7.

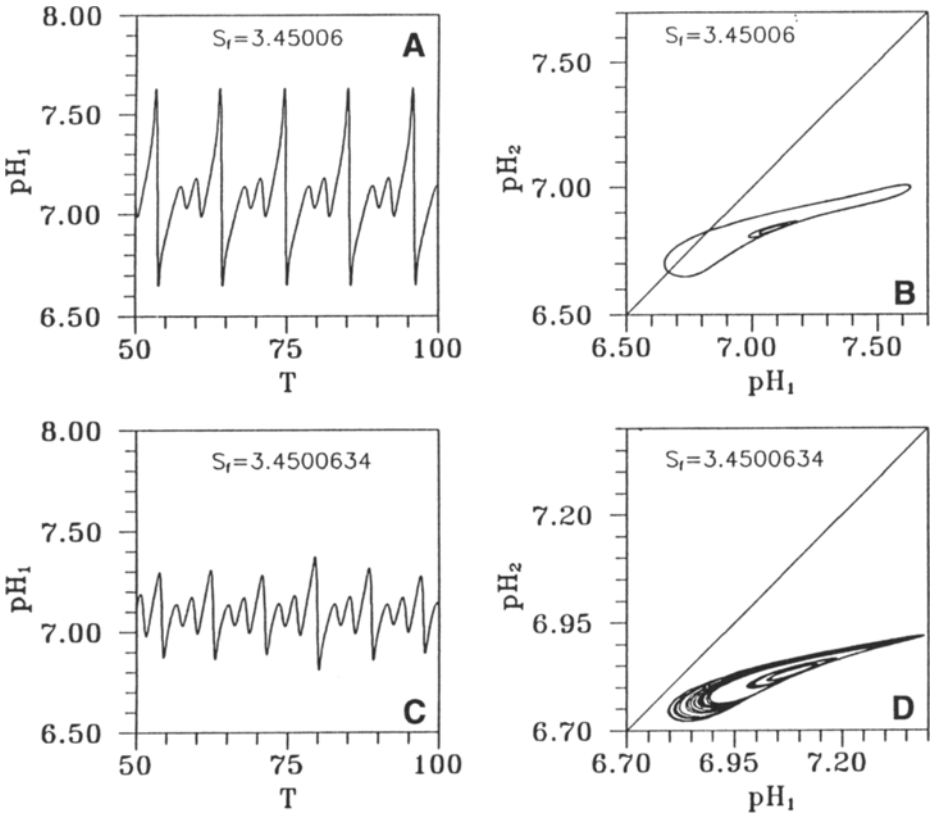

Fig. 18. Dynamic characteristics of two points at the edge of the heavy-density chaotic region: (**A** and **B**) case at s_f = 3.45006 just before the heavy-density region: (**C** and **D**) case at s_f = 3.4500634 just at the beginning of the heavy density chaotic region.

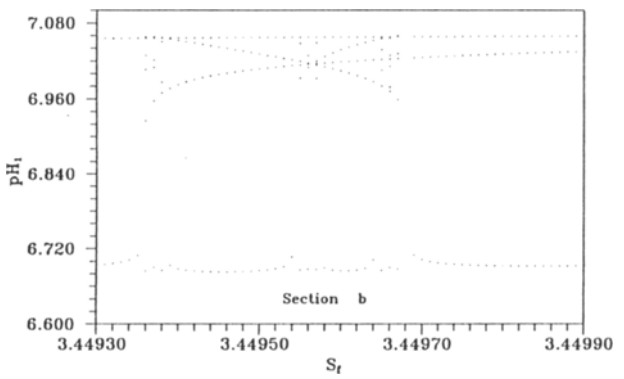

Fig. 19. Enlargement of the relatively wide periodic windows in Fig. 6 section b.

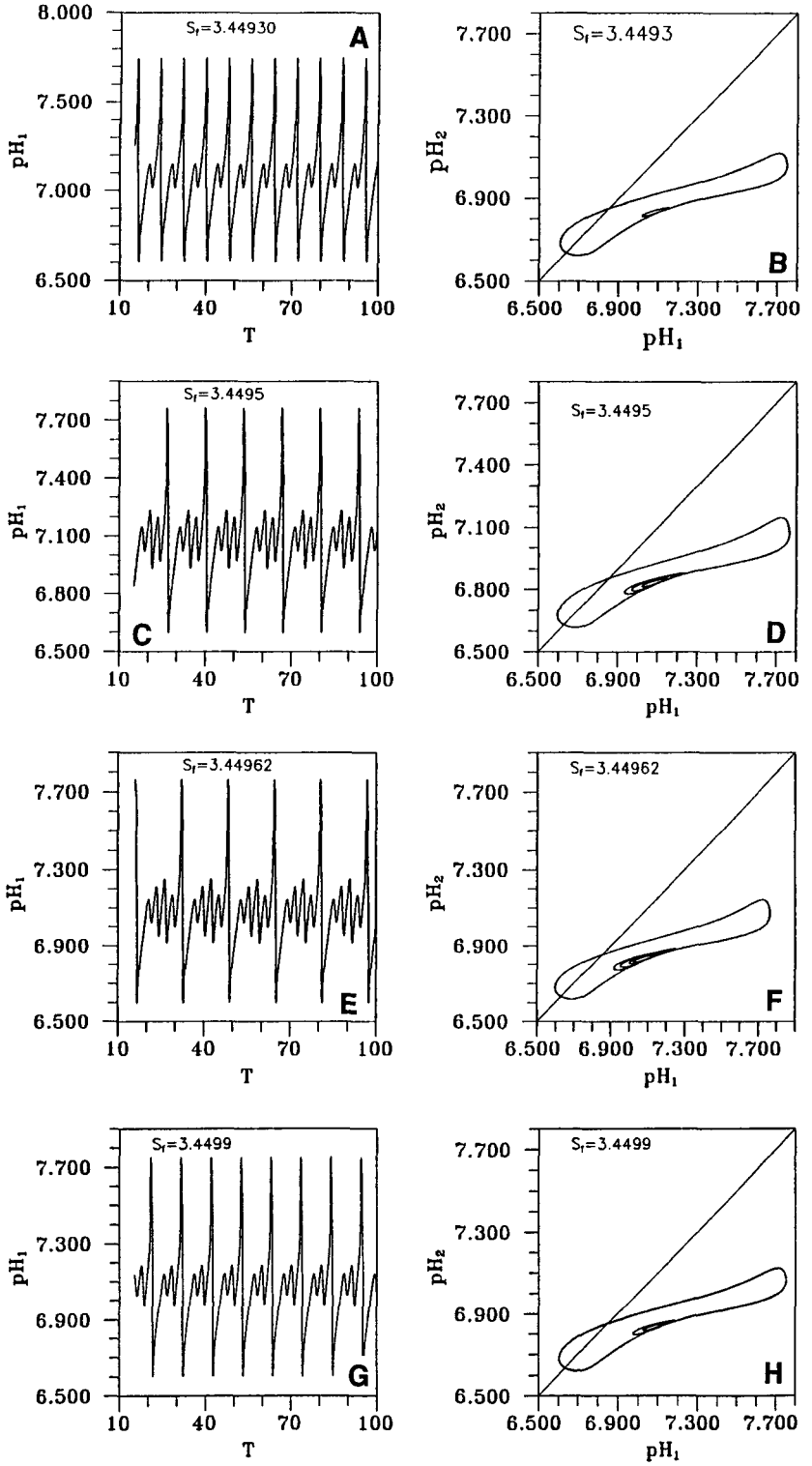

Fig. 20. Dynamic characteristics of four periodic windows: (**A** and **B**) Case of P_2 at s_f = 3.4493. (**C** and **D**) Case of P_4 at s_f = 3.4495. (**E** and **F**) Case of P_5 at s_f = 3.44962. (**G** and **H**) Case of P_3 at s_f = 3.4499.

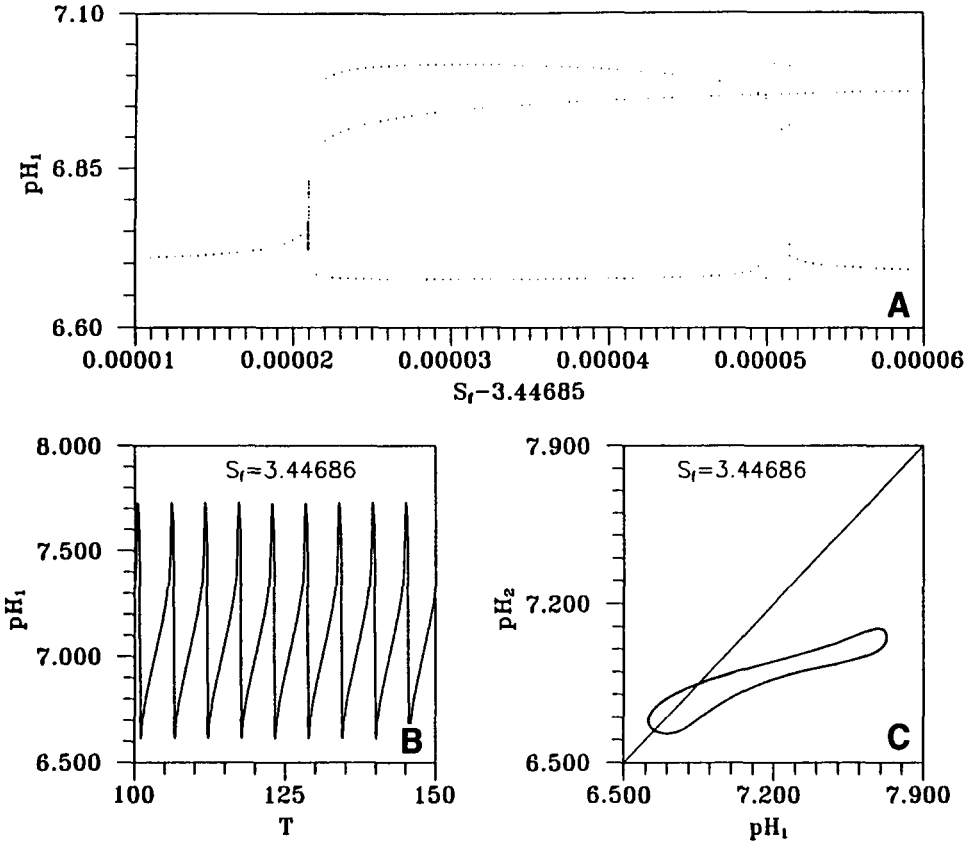

Fig. 21. Dynamic characteristics of section (C): (**A**) Enlargement of section C in Fig. 6. (**B** and **C**) Case of P_1 at s_f = 3.44686.

tions of the complex dynamic analysis in physiological processes was recently published by Elbert et al. (*56*).

The intrinsic oscillatory behavior presented in this article is in agreement with the experimental observations of Friboulet et al. (*9*), who have shown the in vitro oscillations in potential differences between two compartments separated by an artificial acetylcholinesterase membrane when one of the two compartments is injected by acetylcholine substrate.

CONCLUSIONS

A simple and phenomenological two-compartment model is used to investigate the complex dynamic characteristics of an enzyme system inhibited by substrate and affected by the production of hydrogen ions, where the enzyme exists free in solution in each compartment. The system is mathematically described by four differential equations and 11 parameters. The substrate feed concentration (s_f) is selected by the bifurcation

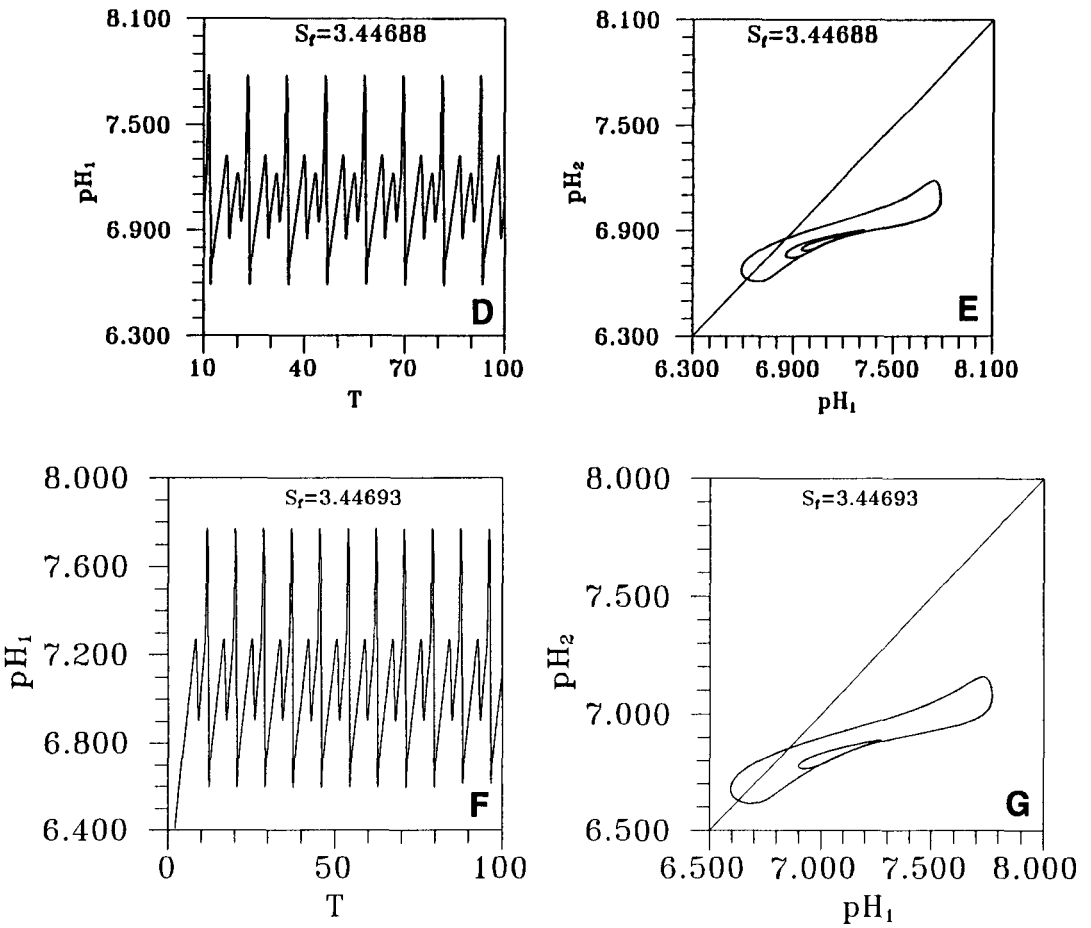

Fig. 21. (cont'd). (**D** and **E**) Case of P_3 at s_f = 3.44688. (**F** and **G**) Case of P_2 at s_f = 3.44693.

parameter. Five of the other 10 parameters are fixed at values used earlier by El-Nashaie et al. (42). The remaining five parameters are chosen at values in the vicinity of the degenerate Hopf bifurcation point denoted by (a) in Fig. 2. In the vicinity of this base set of values of the parameters, a pH_1-s_f bifurcation diagram has been obtained. This diagram is characterized by the existence of four HB points at low substrate concentrations. The four HB points are connected by two periodic branches, creating a bistability phenomenon in certain regions of bifurcation parameter where a periodic and a point attractor coexist with the unstable limit cycle acting as sepaatrices. The transition from the small-amplitude oscillation emerging from the HB_4 point to the relatively large-amplitude oscillation proved to be quite complex. As s_f decreases, a period doubling sequence leading to banded chaos is observed followed by fully developed chaos at crisis points. The fully developed chaos bifurcates to the P_3 window by a tangent

bifurcation mechanism. The P_3 attractors lose their stability to give three-band chaos followed by fully developed chaos. As s_f decreases, this fully developed chaos bifurcates to the P_6 window by the tangent bifurcation mechanism. The P_6 windows bifurcate to three-band chaos by a period doubling mechanism. The heavy-density chaotic region disappears completely close to point $s_f = 3.4500624$; the three-banded chaos turns to intermittency again and loses its stability to a P_3 attractor. The heavy-density chaotic region is interrupted by some narrow periodic windows (P_3, P_5, and P_6 windows).

It is interesting to note that many of the dynamic phenomena discovered by Holden and Fan (*17–20*) using the three-dimensional nonphenomenological action potential Rose-Hindmarsh model are also obtained using the present phenomenological two-compartment model.

A variety of the dynamical modes characterizing this enzyme system have been presented using the nonlinear dynamic approach. The results relate to some physiological processes, especially the self-excitation of some of the smooth muscle activated by acetylcholine-acetylcholinesterase reaction (*10*).

REFERENCES

1. Blumenthal, R., Chongeux, J. P., and Leefever, R. (1970), *J. Membrane Biol.* **2,** 351.
2. Offner, F. F. (1972), *J. Biophys.* 1583.
3. Arndt, R. A. and Roper, L. O. (1975), *J. Theor. Biol.* 249.
4. Grasman, J. (1984), *Bull. of Math. Biol.* **46,** 407.
5. Wang, L. P., Pichler, E. E., and Ross, J. (1990), *Proc. Natl. Acad. Sci. USA* **97,** 9467.
6. Canavier, C. C., Clark, J. W., and Byrne, J. H. (1990), *J. Biophys.* **57,** 1245.
7. Fuchikami, N., Sawashima, N., Naito, M., and Kambara, T. (1993), *Biophys. Chem.* **46,** 249.
8. Doyon, B. (1992), *Acta Biotheor.* **40,** 113.
9. Friboulet, A., David, A., and Thomas, D. (1981), *J. Membrane Sci.* **8,** 33.
10. Guyton, A. C. (1986), in *Medical Physiology,* 7th ed., W. B. Saunders Company, pp. 137, 551–553, 682.
11. Canovas-Munoz, M. D., Munoz-Delgado, E., and Vidal, C. J. (1991), *Biochem. Biophys. Acta.* **1076,** 259.
12. Koch, A. L. (1986), *J. Theor. Biol.* 120.
13. Goldman, R., Silman, I., Caplan, S. R., Kedem, O., and Katchlski, E. (1965), *Science* **150,** 758.
14. Hindmarsh, J. L. and Rose, R. M. (1982), *Nature* **296,** 162.
15. Hindmarsh, J. L. and Rose, R. M. (1984), *Proc. Roy. Soc.* **B221,** 87.
16. Fitzhugh, R. (1961), *Biophys. J.* **1,** 445.
17. Holden, A. V. and Fan, Y. S. (1992), *Chaos, Solitons and Fractals* **2,** 221.
18. Holden, A. V. and Fan, Y. S. (1992), *Chaos, Solitons and Fractals* **2,** 349.

19. Holden, A. V. and Fan, Y. S. (1992), *Chaos, Solitons and Fractals* **2,** 583.
20. Fan, Y. S. and Holden, A. V. (1993), *Chaos, Solitons and Fractals* **3,** 439.
21. Ray, W. H. (1977), in *App. of Bifurcation Theory,* Rabinowitz, P. H., ed., Academic, New York, p. 285.
22. Bailey, J. E. (1977), *Chemical Reactor Theory,* Prentice-Hall, Englewood Cliffs, NJ, p. 758.
23. Ruelle, D. (1980), *Math. Intell.* **2,** 126.
24. Feigenbaum, M. J. (1980), *Los Alamos Sci.* **1,** 4.
25. Hudson, J. L. and Mankin, J. C. (1981), *J. Chem. Phys.* **74,** 6171.
26. Lorenz, E. N. (1980), *Ann. NY Acad. Sci.* **357,** 282.
27. Roux, J. C., Rossi, A., Bachelart, S., and Vidal, C. (1980), *Phs. Lett.* **7A,** 391.
28. Simoyi, R. H., Wolf, A., and Swinney, H. L. (1982), *Phy. Rev. Lett.* **49,** 245.
29. Arecchi, F. T., Meucci, R., Puccioni, G., and Tredicce, J. (1982), *Phys. Rev. Lett.* **49,** 1217.
30. Libchaber, A., Laroche, C., and Fauve, S. (1982), *J. de Phys. Lett.* **43,** 211.
31. Jorgensen, D. V. and Aris, R. (1983), *Chem. Eng. Sci.* **38,** 45.
32. Jorgensen, D. V., Farr, W. W., and Aris, R. (1984), *Chem. Eng. Sci.* **39,** 1741.
33. Chemburkar, R. M., Rossler, O. E., and Varma, A. (1987), *Chem. Eng. Sci.* **42,** 1507.
34. Lynch, D. T. (1992), *Chem. Eng. Sci.* **47,** 347.
35. Teymour, F. and Ray, W. H. (1992), *Chem. Eng. Sci.* **47,** 4133.
36. El-Nashaie, S. S. E. H., Abashar, M. E., and Teymour, F. A. (1993), *Chaos, Solitons, and Fractals* **3,** 1.
37. May, R. M. (1976), *Nature* **261,** 459.
38. Hassell, M. P., Comins, H. N., and May, R. M. (1991), *Nature* **353,** 255.
39. Havacek, V. and Van Rompay, P. (1981), *Chem. Eng. Sci.* **36,** 1587.
40. Nicolis, G., Erneux, T., and Herschhowitz, M. (1978), *Adv. Chem. Phys.* **38,** 263.
41. Li, R. S. and Nicolis, G. (1981), *J. Phys. Chem.* **85,** 1912.
42. El-Nashaie, S. S. E. H., Ibrahim, G., and El-Refaie, M. A. (1983), *Appl. Biochem. Biotechnol.* **8,** 275.
43. Nandapurkar, P. and Hlavacek, V. (1984), *Bull. of Math Biol.* **46,** 269.
44. Thomas, D. R., Zhuo-Cheng, Y., and Lee-Wah, Y. (1986), *J. Math. Biol.* **23,** 263.
45. Alexander, J. C. (1986), *J. Math. Biol.* **23,** 205.
46. Cleave, J. P., Levine, M. R., Fleming, P. J., and Long, A. M. (1986), *J. Theor. Biol.* **119,** 299.
47. Novak, B. and Laszlo, E. (1985), *J. Theor. Biol.* **120,** 309.
48. El-Nashaie, S. S. E. H., Ibrahim, G., and El-Rifaie, M. A. (1983), *Appl. Biochem. Biotechnol.* **8,** 467.
49. El-Nashaie, S. S. E. H., Ibrahim, G., and El-Shishini, S. S. (1984), *Appl. Biochem. Biotechnol.* **9,** 455.
50. Doedel, E. J. (1986), *AUTO: Software for Continuation and Bifurcation Problems in Ordinary Differential Equations,* California Institute of Technology, Pasadena, CA.
51. Pewtzold, L. R. (1983), "Differential Algebraic Solver," Applied Mathematics Division, 8331 Sandia Nat. Lab., Livermore, CA, 94,550.
52. Planeaux, J. B. and Jensen, K. F. (1986), *Chem. Eng. Sci.* **41,** 1497.

53. Glass, L. and Mackety, M. C. (1988), in *From Clocks to Chaos, The Rhythm of Life,* Princeton University Press, Princeton, NJ, p. 44.
54. Pomeau, Y. and Manneville, P. (1980), *Commun. Math. Phys.* **74,** 189.
55. Lopes-da-Silva, F. (1992), *Neurosci. Lett.* **143,** 4.
56. Elbert, T. Ray, W. J., Kowalik, Z. J., Skinner, J. E., Graf, K. E., and Birbaumer, N. (1994), *Physiol. Rev.* **74,** 1.